Spring 2011

Computational modeling of the combustion and gasification zones in a downdraft gasifier

Marta Ann Muilenburg
University of Iowa

COMPUTATIONAL MODELING OF THE COMBUSTION AND GASIFICATION ZONES IN A DOWNDRAFT GASIFIER

by
Marta Ann Muilenburg

A thesis submitted in partial fulfillment
of the requirements for the Master of
Science degree in Mechanical Engineering
in the Graduate College of
The University of Iowa

May 2011

Thesis Supervisor: Assistant Professor Albert Ratner

Graduate College
The University of Iowa
Iowa City, Iowa

CERTIFICATE OF APPROVAL

MASTER'S THESIS

This is to certify that the Master's thesis of

Marta Ann Muilenburg

has been approved by the Examining Committee for the thesis requirement for the Master of Science degree in Mechanical Engineering at the May 2011 graduation.

Thesis Committee: _____
Albert Ratner, Thesis Supervisor

_____
James Buchholz

_____
Pablo Carrica

ACKNOWLEDGMENTS

I would like to thank Professor Albert Ratner for his belief in my completion of my degree. I would also like to thank the University of Iowa Power Plant for their financial support for the duration of my project. Both of these resources were invaluable when it came to my ability to bring about these results. Finally, I would like to thank my family for all their love and support from the beginning of time, and their unrelenting faith in my "process".

ABSTRACT

Computational modeling was completed on a simplified downdraft gasifier to be implemented at the University of Iowa Oakdale Power Plant. The model was created in Gambit and exported to FLUENT, a computational fluid dynamics software program, in order to model non-premixed combustion on biomass fuels and better understand the combustion and gasification zones.

The fuels were modeled as coal particles with an empirical formula for biomass derived from off-site proximate and ultimate analyses. The coal model inherent to FLUENT contains the same atomic species (C, H, N, O, and S) as the biomass tested. The model was tested for varying packing densities, oxidizer inlet velocities and fuel type to describe the effects on the combustion zone.

It was concluded that packing densities around 0.5 with oxidizer inlet velocities less than 5 m/s would be ideal for modeling wood. The temperature distribution was the most even in this environment and produced a large, rich fuel combustion (RFC) zone where gasification and pyrolysis could occur.

The different fuels were found to have similar temperature and mean mixture fraction patterns, although the maximum temperatures attained were very different (1080K for seed corn vs. 678K for wood), the wood showed a greater area of RFC for gasification and pyrolysis.

TABLE OF CONTENTS

LIST OF TABLES

LIST OF FIGURES

LIST OF NOMENCLATURE

a	Absorption coefficient
C_x	Constant
c_p	Specific heat
F	Body forces
f	Mixture fraction
G	Incident Radiation
G_b	Generation of turbulent kinetic energy due to buoyancy
G_k	Generation of turbulent kinetic energy due to the mean velocity gradient
g	Gravity
H	Total enthalpy
H_j	Enthalpy of species j
h_j^0	Heat of formation
I	Unit tensor
k	Turbulent kinetic Energy
k_t	Turbulent thermal conductivity
m	Mass
n	Refractive index
q_r	Radiation flux
S_x	User defined function
T	Temperature
t	Time
v	Velocity
Y_M	Fluctuating dilatation

Y_j	Mass fraction of species j
Z_i	Elemental mass fraction of species i
ε	Dissipation rate of turbulent kinetic energy
μ	Molecular viscosity
μ_t	Turbulent viscosity
ρ	Density
σ	Stefan-Boltzmann constant
$\bar{\tau}$	Stress tensor
$\bar{\Phi}_i$	Mean scalar quantities

CHAPTER 1

INTRODUCTION

As we learn more about the hazardous effects of our current energy production demographic, it has become increasingly important to find new ways to produce energy. In 2005, the United States alone consumed 100 quadrillion BTU's (29 PWh) of energy, 86% of which came from fossil fuels (U.S. Department of Energy, 2011). Burning fossil fuels releases harmful chemicals into the atmosphere that have direct and indirect negative impacts on living organisms, including trapping heat and other molecular compounds that contribute to acid rain. Although efforts to find cleaner energy sources have improved over the last 6 years, they only increased from an estimated 15.7% in 2005 to 17% in 2009 (U.S. Department of Energy, 2011).

One area of increased research is biomass. Biomass includes organic material ranging from wood and crops to animal excrement and post production waste from industrial plants. Uses for these products include creating biofuels such as ethanol, produced by the fermentation of sugars in wheat, corn, and potatoes. However, biomass research also includes direct combustion and gasification techniques as possible energy supplies for the future.

Biomass combustion is currently being utilized around the world to supplement fossil fuel power plants. The University of Iowa Power Plant modified boiler 11 in 2003 to burn a mixture of coal and biomass at a rate of 170,000 lbs/hr (The University of Iowa, 2007). This redesign produced not only a $500,000 per year savings for the university, but also reduced the CO_2 output by more than 50,000 tons per year and displaced 30,000 tons of coal per year by co-firing oat hulls purchased from Quaker Oats in Cedar Rapids,

IA. Adding to the reduced CO_2 emissions, this co-fire design has reduced NO_x, SO_2, CO, and particulate emissions as well.

The University of Iowa Power Plant is constantly looking for ways to do their part in reducing the carbon footprint of the university. In 2011, the University of Iowa Oakdale Power Plant (UIOPP) is in the process of replacing an old boiler with a more efficient Hearst biomass boiler and a gasifier from AgBio in Tama, IA. This gasifier will be used for research purposes for potential future use on campus.

1.1 Types of Gasifiers

While there are many different gasifier designs, they are generally grouped into 3 different types: Fixed or Updraft (UD), Fluidized Bed (FB), and Entrained Flow (EF). The AgBio gasifier is an EF design.

A UD gasifier is fed through an opening at the top and piles the mass on a divider close to the bottom (Figure 1.1) (U.S. Department of Energy). Steam, oxygen, or air enter from an inlet at the bottom and rise up through the mix with material sifting down through the divider plate. Near the divider plate, combustion between the oxidants and the material occurs and the gasifier sees its highest temperatures. Above the combustion zone is the gasification zone, carbonization zone, and drying zone, in ascending order seen in Figure 1.2 (Ulstad, 2010). Each zone is a vital component to the gasification process that will be discussed later. The gasification products are vented through the side near the top of the gasifier, being carried with the "updraft", while the ash and char are deposited out the bottom.

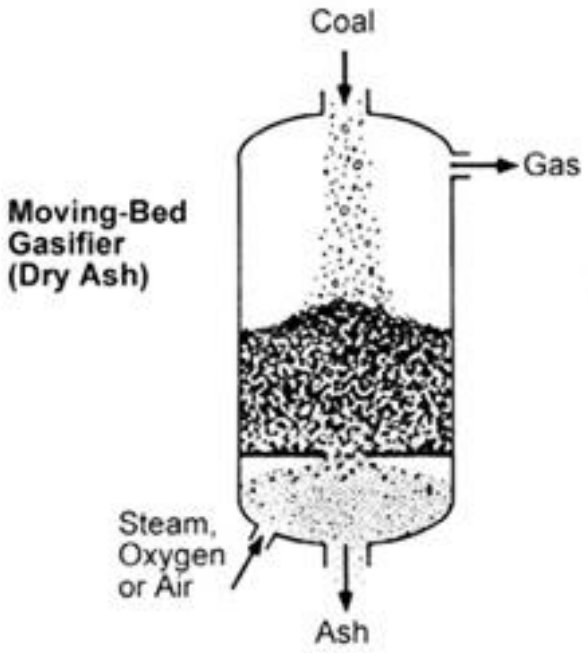

Figure 1.1Updraft Gasifier

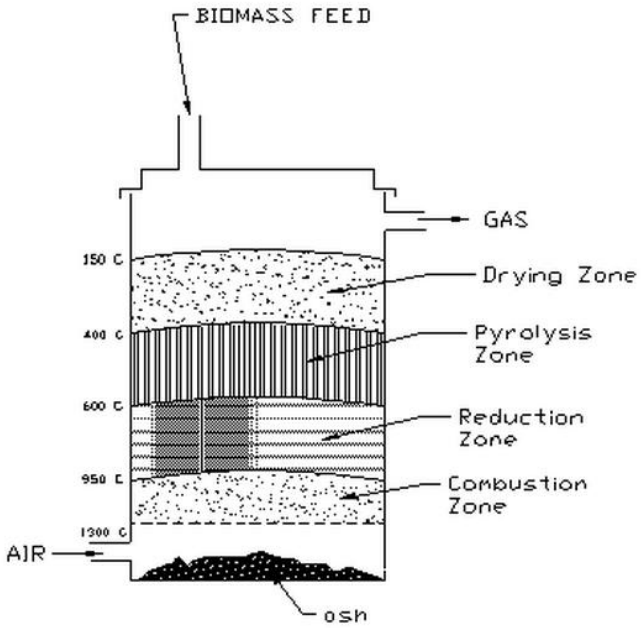

Figure 1.2 Zone design for a UD Gasifier

Similar to a UD, FB gasifier oxidants, ash and char enter and exit through the bottom of the gasifier as seen in Figure 1.3 (U.S. Department of Energy). However, a FB gasifier draws the mass in from the side of the gasifier and the products are vented through the top. Instead of seeing different process zones, the FB gasifier utilizes back-mixing. Particles that are partially gasified are mixed with new feeder particles and the temperatures do not get as high as in the combustion zone of the UD gasifier.

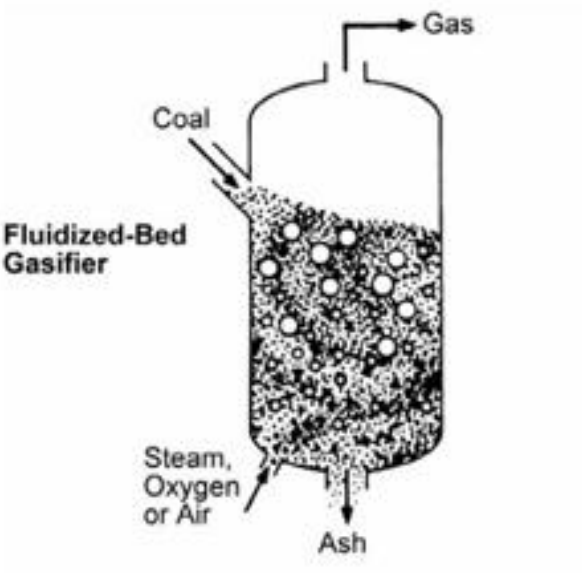

Figure 1.3 Fluidized bed gasifier

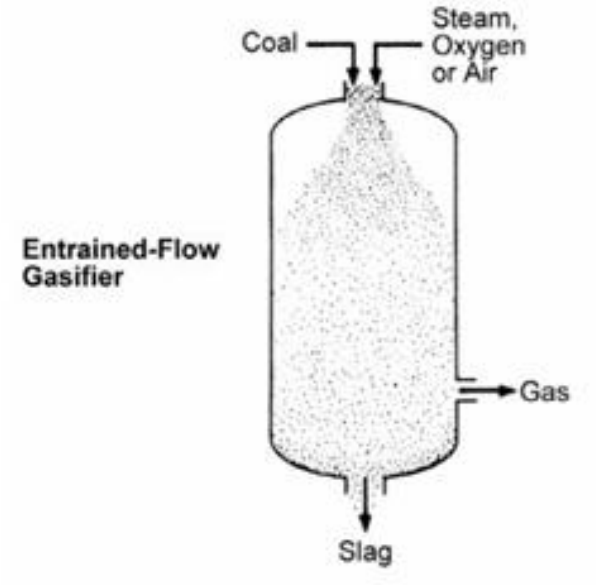

Figure 1.4 Entrained flow gasifier

The EF gasifiers (Figure 1.4) have their mass flow and air, steam, or oxygen inlet on the top (U.S. Department of Energy). The mass particles are surrounded (or entrained) by the oxidant as the mass moves through the gasification process. EF gasifiers are able to operate at very high temperatures and are able to create very little inert ash and char at the end of the process which then exits the system through the bottom. The products of gasification are vented through the side of the gasifier near the bottom or through the ash and char.

The AgBio design, a mixture of the EF and FB gasifiers, has a separate air inlet and biomass inlet at the top that both feed into a center fire tube. A bottom tray that is larger in diameter than the fire tube collects the ash and char and allows the products to travel through this area out of the fire tube and into a surrounding chamber. The gases are then vented out of this chamber to be burned in the Hearst boiler. The current design can be seen in Figure 1.5.

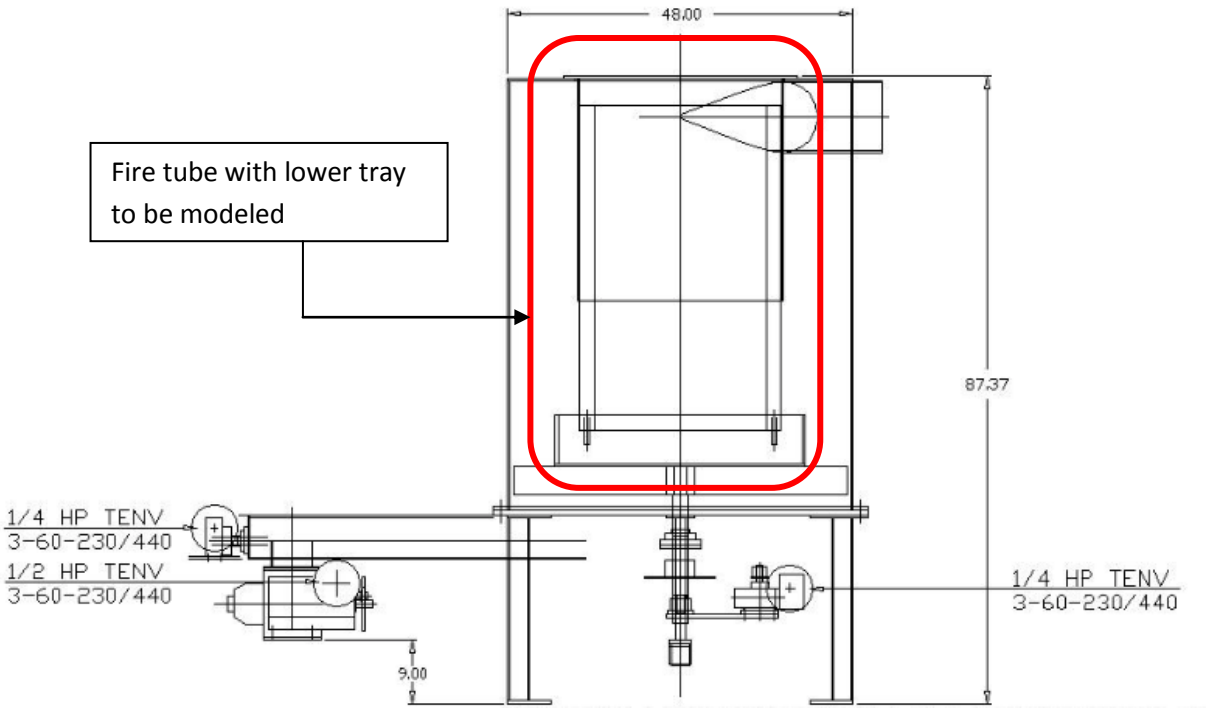

Figure 1.5 AgBio gasifier design drawing (in inches)

1.2 Gasification Process

As mentioned in the designs of the various types of gasifiers, there are many components to the gasification of biomass materials for use as an energy source. However, there are always four main zones which can be classified as: drying, pyrolysis, combustion, and gasification.

Equation 1.1 shows an example of a simple combustion reaction between methane and oxygen. While this reaction does exist in small quantities during the gasification process, it is merely a representation of the breakdown of hydrocarbons with an oxidant during combustion and the bi-products produced.

$$CH_4 + 2O_2 \rightarrow CO_2 + 2H_2O \qquad (1.1)$$

Biomass chemical make-up is much more complex than methane, as determined through ultimate and proximate analysis done by an outside lab. Modeling the chemical decomposition of biomass during combustion involves complicated devolatization mechanisms resulting in a mixture of methane (CH_4), water, carbon monoxide (CO), carbon dioxide (CO_2), tar, ash, and pure hydrogen (H_2). During the drying process it is assumed the biomass liquid water content is transformed into water vapor.

In the pyrolysis zone, volatiles are released from their solids (Equations 1.2) and are broken down further shown in Equation 1.3 (Cornejo & Farias, 2011). These reactions take place around 773K.

$$Biomass_s \rightarrow Char_s + Volatiles_s + Steam_g \quad (1.2)$$

$$Volatiles \rightarrow \alpha_1 CH_4 + \alpha_2 CO + \alpha_3 CO_2 + \alpha_4 H_2 + \alpha_5 H_2O \quad (1.3)$$

Since there is no data on the exact distribution of the volatiles in biomass, they were predicted using Equation 1.4, where *VOL* indicates the total volatile content of the biomass, based on the dry proximate analysis of each biomass (Cornejo & Farias, 2011). The coefficients and predicted species distributions for each biomass can be seen in Tables 1.1 and 1.2, respectively. These equations are used under the assumption that the biomass materials are modeled as coal particles with their empirical formula changed to match the make-up of the biomass. This assumption is a generalization and leads to expected compositions that are negative, particularly in the species involving carbon. This would be expected as coal has a much lower volatiles content (around ½ the content of wood) and higher fuel to oxygen ratios (3:1 compared to 1:1) (Stull, 2003).

$$Species = a - b * VOL + c * VOL^2 \quad (1.4)$$

Table 1.1 Species distribution coefficients

	a	*b*	*c*
CH_4	0.21	0.469	0.241
H_2	0.157	0.868	1.338
CO_2	0.135	0.9	0.196
CO	0.425	2.653	1.906
H_2O	0.409	2.389	4.554

Table 1.2 Predicted species composition of biomass materials

	Wood	**Seed Corn**
CH4	-0.016	-0.006
H2	0.417	0.252
CO	-0.501	-0.426
CO2	-0.439	-0.494
H2O	1.786	1.153

The model being used in this research implements a devolatization that is generated by FLUENT using a probability density function (PDF) determined by the ultimate and proximate analysis of the biomass tested. These figures give an example of how the data would be calculated were the PDF not used.

The combustion zone operates at approximately 1123K (Atnaw & Sulaiman, 2009) and is governed by Equations 1.5 – 1.8 (Cornejo & Farias, 2011). These include, in order, the water-gas shift reaction, CO combustion, H_2 combustion, and CH_4 combustion.

$$CO + H_2O \leftrightarrow CO_2 + H_2 \quad (1.5)$$

$$CO + O_2 \rightarrow 2CO_2 \quad (1.6)$$

$$2H_2 + O_2 \rightarrow 2H_2O \quad (1.7)$$

$$CH_4 + 2O_2 \rightarrow CO_2 + 2H_2O \quad (1.8)$$

The water-gas shift reaction is a reversible reaction while the others are only reacting one direction. Each of these reactions contributes to the increased creation of CO_2 and H_2.

Gasification can occur in any of the zones but is prevalent in the gasification zone due to the lack of oxidizer (discussed later). This process can be carried out at a range of temperatures, from 400 to 1500K (Ulstad, 2010), and consists of char combustion and the gasification of char with steam and CO_2, as well as limited pyrolysis reactions (Reed & Desrosiers, 1979). These reactions increase the amount of CO, CO_2 and H_2 produced by the process. Therefore, limiting the amount of char produced by using biomass over coal would indicate a reduction in the CO_2, CO, and H_2, output. Although the H_2 can be used as a fuel, the reduced CO_2 and CO are desirable outcomes from using biomass as an energy source. These equations can be seen in Equations 1.10 – 1.12.

$$C_{(s)} + O_2 \rightarrow CO_2 \quad (1.10)$$

$$C_{(s)} + H_2O \rightarrow CO + H_2 \quad (1.11)$$

$$C_{(s)} + CO_2 \rightarrow 2CO \quad (1.12)$$

Each of the combustion reactions, including char combustion, relies on the fact that there will be enough O_2 to oxidize the fuel and complete the reaction. This fuel to air

ratio is referred to as the equivalence ratio (ER). The ER diagram shown in Figure 1.6 shows the relationship of combustion, gasification, and pyrolysis for a biomass of empirical formula $CH_{1.4}O_{0.6}$ (Reed & Desrosiers, 1979). Although the biomass modeled herein does not have this exact formulation, the overall effect is expected to be similar.

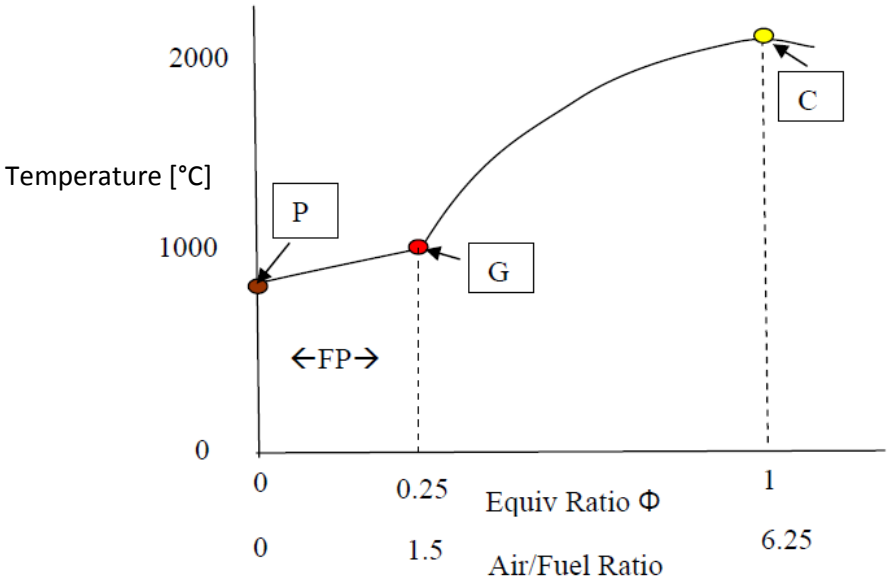

Figure 1.6 Equivalence ratio diagram of biomass $CH_{1.4}O_{0.6}$

The values on the vertical axis indicate the temperature in °C that could be reached for a dry, ash-free biomass material. The maximum temperature indicated for combustion (C) is approximately 2025°C (2298K) at an ER of 1, which decreases with the inclusion of water and ash in the material being utilized. Conventional gasification (G) takes place at an ER of approximately 0.25 while pyrolytic gasification (P) occurs at an ER at or near to 0. Starved of oxidizer, the material is devolatized by the high temperatures from the combustion zone transferred by radiation and convection.

The purpose of this research is to model the combustion and gasification zones in a downdraft gasifier. These results will be used to install monitors on the AgBio gasifier at the UIOPP and to maximize the efficiency of the output gases.

CHAPTER 2

MODELING

2.1 Design

ANSYS FLUENT and Gambit software was used to model the down-draft gasifier system to be installed at UIOPP. While some researchers have utilized the multiphase model in FLUENT (Cornejo & Farias, 2011; Yimlaz, et al., 2010), others have modeled the process with mathematical user defined functions (Watanabe & Otaka, 2006; Paes, 2005; Huang & Ramaswamy, 2009; Cuoci, et al., 2009; Wen & Chaung, 1979). Still others have broken down their modeling by zone, i.e. drying (Ciegis & Starikovicius, 2002) or pyrolysis (Babu & Chaurasia, 2003). Although most work has focused on the gasification of coal particles (Watanabe & Otaka, 2006; Wen & Chaung, 1979; Cuoci, et al., 2009; Cornejo & Farias, 2011; Yilmaz, et al., 2010), some have focused on biomass materials (Paes, 2005; Huang & Ramaswamy, 2009; Ciegis & Starikovicius, 2002; Babu & Chaurasia, 2003). The model chosen for this research focuses on the combustion zone of biomass in a down-draft gasifier. The combustion zone determines the temperatures in the gasifier and the reactions in the other zones and is therefore pivotal in the gasification process.

Gambit was used to create a two-dimensional model of the fire tube in the AgBio gasifier. Figure 2.1 shows the model created with the completed mesh. FLUENT was then used to set the parameters of the model. The model uses an oxidizer inlet at the top but relocates the fuel input to the approximate fill height of 12” above the bottom plate. The fuel inlets are on both sides and are 6” wide. This was done to simulate the pile of material at the bottom of the gasifier at an even level. The bottom of the gasifier is made of steel that is defined as a trap (particles stick to the surface) and the walls, also made of

steel, are reflective. The gas escapes through 3" tall openings at the base of each wall with a defined temperature of 300K and backflow normal to the boundary. This design was modified from the actual design of the gasifier for simplification in processing and to correct for combustion at the oxidizer input.

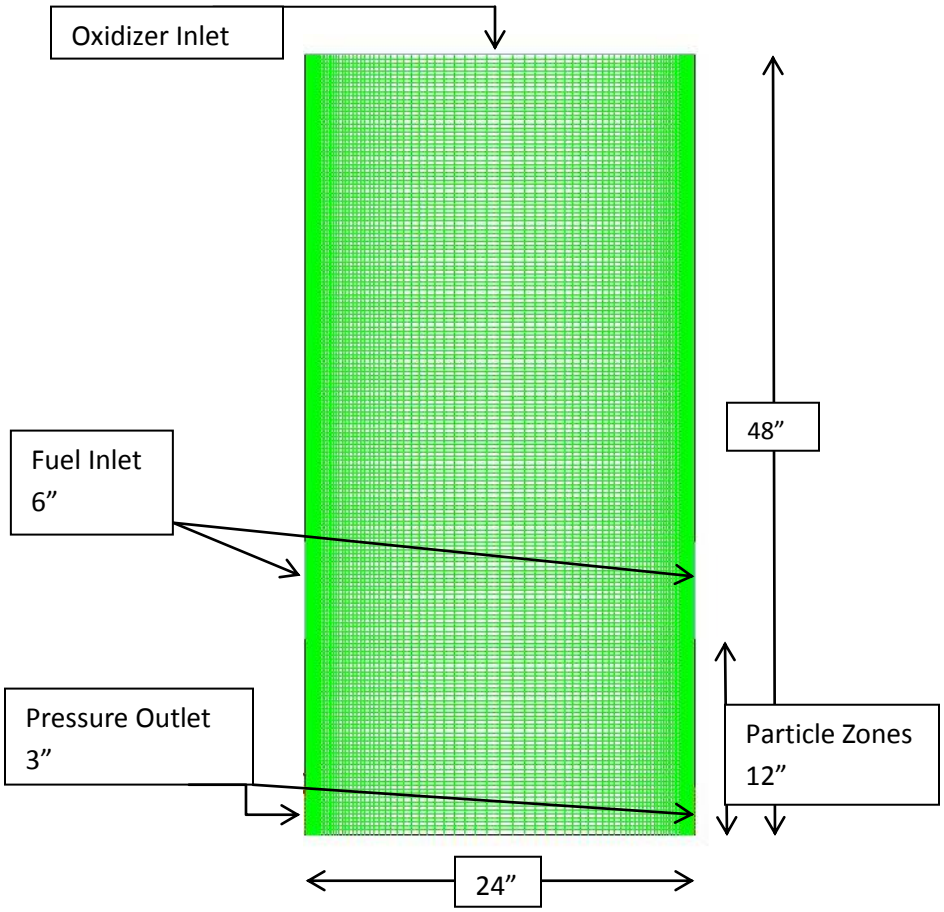

Figure 2.1 Gambit mesh model of downdraft gasifier

The model is operated at standard pressure with an oxidizer inlet temperature of 300K, fuel inlet temperature of 400K, and employing the solution methods shown in Table 2.1. All other solution methods are First Order Upwind.

Table 2.1 Solution methods

	Solution Method
Pressure-Velocity Coupling Scheme	SIMPLE
Gradient	Least Squares Cell Based
Pressure	PRESTO!

2.2 Governing Equations

Non-premixed combustion was chosen as the solver for this study. Every flow model in FLUENT solves the conservation of mass and momentum as seen in Equations 2.1 and 2.2.

$$\frac{\partial \rho}{\partial t} + \nabla \cdot (\rho \vec{v}) = S_m \tag{2.1}$$

$$\frac{\partial}{\partial t}(\rho \vec{v}) + \nabla \cdot (\rho \vec{v} \vec{v}) = -\nabla p + \nabla \cdot (\bar{\tau}) + \rho \vec{g} + \vec{F} \tag{2.2}$$

$$\bar{\tau} = \mu \left[\left(\nabla \vec{v} + \nabla \overrightarrow{v^T} \right) - \frac{2}{3} \nabla \cdot \vec{v} I \right] \tag{2.3}$$

Equation 2.3 describes the stress tensor. The energy equation was solved for as well, using Equation 2.4. This version of the energy equation is used for non-adiabatic non-premixed combustion problems as the viscous dissipation appears in the S_h term, as necessary, but is neglected in models that are pressure-based as viscous heat transfer is often determined to be negligible in these cases.

$$\frac{\partial}{\partial t}(\rho H) + \nabla \cdot (\rho \vec{v} H) = \nabla \cdot \left(\frac{k_t}{c_p} \nabla H \right) + S_h \tag{2.4}$$

The conduction and species terms from the standard energy equation are combined in the first term on the right hand side of the equation in this model where the total enthalpy, is defined as the sum of the mass fraction and enthalpy for the j^{th} species (Equation 2.5).

$$H = \sum_j Y_j H_j \tag{2.5}$$

H_j is defined as,

$$H_j = \int_{T_{ref,j}}^{T} c_{p,j} dT + h_j^0(T_{ref,j}) \tag{2.6}$$

where $h_j^0(T_{ref,j})$ is the enthalpy of formation of species j at the j^{th} reference temperature. This term negates the need for the heat of reaction source term since the heat of formation is included. However, the energy equation for this model does include a radiation source term. The radiation source term is defined in Equation 2.7.

$$-\nabla \cdot q_r = aG - 4an^2\sigma T^4 \tag{2.7}$$

The species transport solution is solved using the Favre (density-based) mean mixture fraction, $\bar{f}$ (Equation 2.7) and the conservation of the mixture fraction variance, $\overline{f'^2}$ (Equation 2.10).

$$\frac{\partial}{\partial t}(\rho \bar{f}) + \nabla \cdot (\rho \vec{v} \bar{f}) = \nabla \cdot \left(\frac{\mu_t}{\sigma_t} \nabla \bar{f}\right) + S_m \tag{2.8}$$

Where,

$$f = \frac{Z_i - Z_{i,OX}}{Z_{i,fuel} - Z_{i,OX}} \tag{2.9}$$

$$\frac{\partial}{\partial t}\left(\rho\overline{f'^2}\right) + \nabla \cdot \left(\rho\vec{v}\overline{f'^2}\right) = \nabla \cdot \left(\frac{\mu_t}{\sigma_t}\nabla\overline{f'^2}\right) + C_g\mu_t\left(\nabla\bar{f}\right)^2 - C_d\rho\frac{\epsilon}{d}\overline{f'^2} \tag{2.10}$$

Where,

$$f' = f - \bar{f}, \tag{2.11}$$

and $\sigma_t = 0.85$, $C_g = 2.86$, and $C_d = 2.0$.

The ultimate and proximate analyses of the materials for each biomass are entered into the "coal calculator" for the non-premixed combustion model under with the values shown in Tables 2.2 and 2.3, respectively, including the higher heating value (HHV).

Table 2.2 Ultimate and Proximate analysis

	Seed Corn		**Wood**	
	Proximate Analysis	Ultimate Analysis	Proximate Analysis	Ultimate Analysis
Moisture [%]	12.91	-	9.19	-
Carbon [%]	-	44.74	-	49.98
Hydrogen [%]	-	6.28	-	6.02
Nitrogen [%]	-	1.46	-	0.15
Sulfur [%]	-	0.11	-	0.01
Ash [%]	5.21	-	0.74	-
Oxygen [%]	-	47.41	-	43.84
Volatile Matter [%]	74.42	-	79.15	-
Fixed Carbon [%]	7.46	-	10.92	-
HHV [BTU/lb]	8,910	-	8,690	-

This calculator automatically provides the empirical formula, empirical molecular weight, and lower heating value. With the fuel input temperature given, FLUENT calculates a PDF for each material using the above equations, represented in Figure 2.2 with mean mixture fraction on the x-axis, variance on the y-axis, and mean temperature on the z-axis. These equations are used assuming equal diffusivity of each species due to turbulent convection overwhelming molecular diffusion. The PDF is of the form:

$$p(f)\Delta f = \lim_{T\to\infty} \frac{1}{T}\sum_i \tau_i \tag{2.12}$$

In this equation, T is the time scale and τ_i is the amount of time f spends in the Δf. From this look-up table the mean scalar values of mass fraction and temperature can be calculated by the Equation 2.13.

$$\bar{\phi}_i = \int_0^1 p(f)\phi_i(f,\bar{H})df \tag{2.13}$$

The model also uses the standard k-ε turbulence equations seen below (Equations 2.14 and 2.15).

$$\frac{\partial}{\partial t}(\rho k) + \frac{\partial}{\partial x_i}(\rho k v_i) = \frac{\partial}{\partial x_j}\left[\left(\mu + \frac{\mu_t}{\sigma_t}\right)\frac{\partial k}{\partial x_j}\right] + G_k + G_b + \rho\varepsilon - Y_M \tag{2.14}$$

$$\frac{\partial}{\partial t}(\rho \varepsilon) + \frac{\partial}{\partial x_i}(\rho \varepsilon v_i) = \frac{\partial}{\partial x_j}\left[\left(\mu + \frac{\mu_t}{\sigma_\varepsilon}\right)\frac{\partial \varepsilon}{\partial x_j}\right] + C_{1\varepsilon}\frac{\varepsilon}{k}(G_k + C_{3\varepsilon}G_b) - C_{2\varepsilon}\rho\frac{\varepsilon^2}{k} \tag{2.15}$$

The G_b, and Y_M terms are neglected in this case since gravity is considered and dilatation dissipation only occurs at high Mach numbers, which is not under consideration in this model.

$$\mu_t = \rho C_\mu \frac{k^2}{\varepsilon} \tag{2.16}$$

The turbulent viscosity is modeled using Equation 2.16. $C_{1\varepsilon}$, $C_{2\varepsilon}$, and Cμ are all constants defined by FLUENT for air and water to model fundamental turbulent flow and are used in this case. The turbulent Prandlt numbers for k and ε, σ_k and σ_ε, are given as 1.0 and 1.3, respectively. For this model, no user-defined source terms were used.

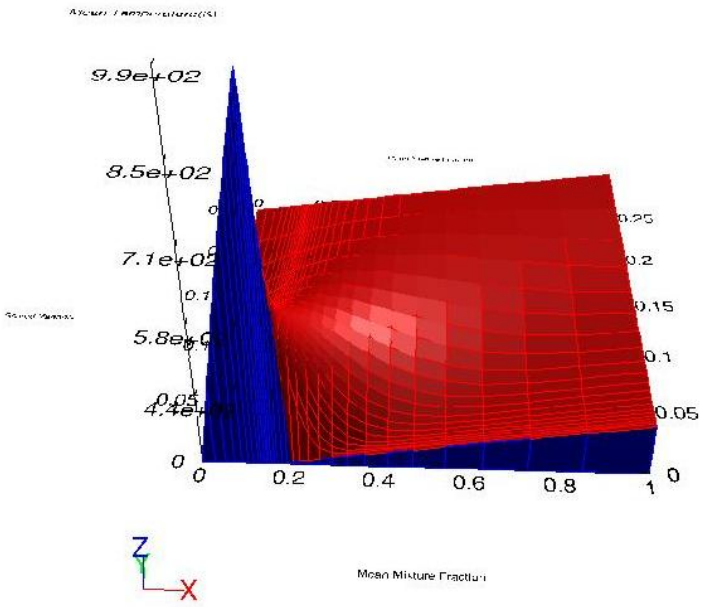

Figure 2.2 PDF 3D look-up table for wood particles

2.3 Variations

Three variables were tested during this experiment: porosity of the particle area, oxidizer inlet velocity, and fuel type.

For the first set of cases, the inlet fuel mass flow rate at 0.25 kg/s, the fuel velocity magnitude from the left side was 1.0 in the x-direction and -0.5 in the y-direction, while the fuel velocity magnitude from the right was set to -1.0 in the x-direction and -0.5 in the y-direction. The oxidizer fuel velocity was set to 1 m/s in the negative y-direction. All of the porous zones were specified to have the direction of porosity in the negative y-direction to coincide with the direction of the air flow.

Case one evaluated a packed bed in the particle zone that would be quite dense, with a porosity of 0.1. This would happen if the fuel particles being used were very small, such as seed corn or sawdust, or if the majority of the particle zone is comprised of char and ash. Case two considered a situation that would have a medium density throughout the particle zone and porosity was set at 0.5. This situation would occur with fuels that had larger particles such as wood chips or coal. The final case porosity was set at 0.8, which would indicate a very low density in the particle zone. Fuels that would produce this sort of porosity would be expected to have large, irregular shaped particles that do not pack down, such as even chopped wood, or sections of rubber such as tires.

The second variable examined held the porosity constant at 0.5. The fuel velocity inlet was also changed to have no y-direction component. All other variables were held constant while the velocity of the oxidizer were taken as 1 m/s in case one, 5 m/s in case two, and 15 m/s in case three.

The third set of cases comprised of holding the porosity constant at 0.5, the oxidizer inlet velocity constant at 1.5 m/s in the negative y-direction, and the fuel inlet

flow rates at 1 kg/s. The left and right fuel velocity magnitudes were 1.0 and -1.0 in the x-direction, respectively.

CHAPTER 3

RESULTS AND DISCUSSION

3.1 Variations in Porosity

The temperature variations due to the porosity can be seen in Figure 3.1. It is of interest that the most and least porous cases show marked similarity in their temperature gradient. Both of these cases show the highest temperatures at the left fuel inlet traveling down towards the bottom of the gasifier along the wall and to the pressure outlet on the left wall. There also appears to be an arc of warmer temperatures, between 400 and 500K moving in the positive x- and y-directions from the left fuel inlet. The porosity of 0.5 has a more even distribution of temperatures throughout the porous zone as seen in 3.1(b). The maximum temperature distribution from the fuel inlet to the pressure outlet is still present but the volume of higher and more evenly distributed temperature gradients is significantly higher.

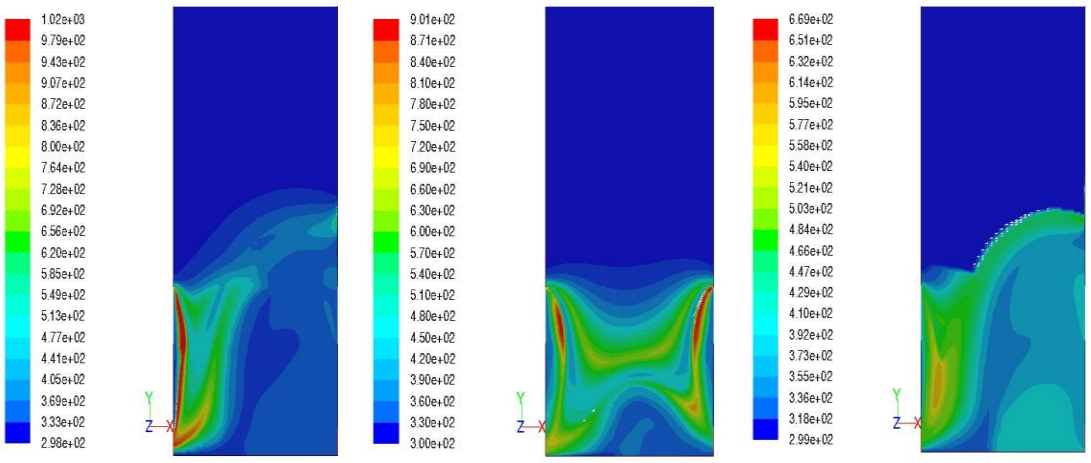

(a) *(b)* *(c)*

Figure 3.1 Temperature gradients with 0.1, 0.5, and 0.8 porosity from left to right

It can also be noted that the maximum temperatures achieved in these cases varies greatly. The maximum temperature of case one is 1020K and case two reaches 901K. Although the difference in the maximum temperature is not great between these two cases the amount of area achieving this temperature is almost double in case one. Case three sees a maximum temperature of 669K, with a temperature gradient post-oxidizer/fuel mixing of 300-600K. This temperature gradient is similar to the gradient seen in case one where the majority of the post-mixture temperature is in the 300-550K. However, case two sees the majority of its post-mixture temperature in the 500-700K range. This indicates that a more even distribution of higher temperatures would be present in cases where there is an even mixture of solid surface to air space, which is expected. The higher temperatures present also increases the chance for gasification and pyrolysis to occur in this zone and indicate that they would occur at a faster rate.

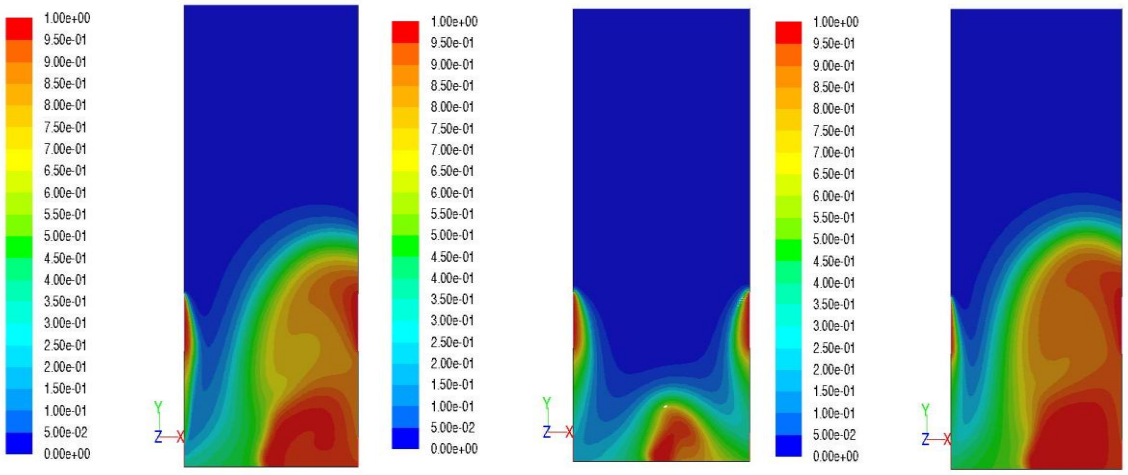

(a) *(b)* *(c)*

Figure 3.2 Mean mixture fraction at 0.1, 0.5, and 0.8 porosity from left to right

Figure 3.2 shows the mixture fraction for each of the porosity cases. Again there appears to be a similarity in the least and most porous cases in terms of the mixture fraction gradient. As seen in Figure 3.2(a) and (c), both cases indicate a large arched pattern in the bottom right of the gasifier extending from the bottom wall to about half the overall height of the gasifier. A mixture fraction of 1.0 indicates all fuel in that zone, 0 indicates all oxidizer. As seen in both case one and three it appears that the particle zone is dominated by unburned fuel and areas of up to half unburned fuel. These models suggest that fuels of very high and very low density would not be ideal in this downdraft gasifier.

Case two shows a very different gradient (Figure 3.2(b)). This image shows small areas of unburned fuel in the middle of the bottom wall and at the fuel inlets. The fuel inlet fuel fraction is expected while the triangular area of unburned fuel at the bottom of the gasifier could be explained by the velocity patterns shown in Figure 3.3. The velocity from the fuel inlet mixes with the downward velocity of the air and creates a vortex at the bottom of the gasifier depositing the unburned fuel there.

Using the previous two sets of data, a stoichiometric combustion line (SCL) can easily be identified. In Figure 3.3, the SCL would lie along the contour of mixture fraction between 0 and greater values, which mimics the temperature gradients from Figure 3.2. Although the temperatures are higher before this contour, the lack of any fuel indicates that all available fuel that has been devolatized and has been burned in lean fuel combustion (LFC). The temperature continues to be high after the flame edge as combustion may be occurring beyond this contour in a rich fuel combustion mode (RFC). Combustion no longer takes place by the time the mixture fraction equals 1.0, indicating all the fuel is remaining in its original state. Referencing Figure 1.6, it would seem that

pyrolysis and gasification have become dominant when the mean mixture fraction has reached approximately 0.75.

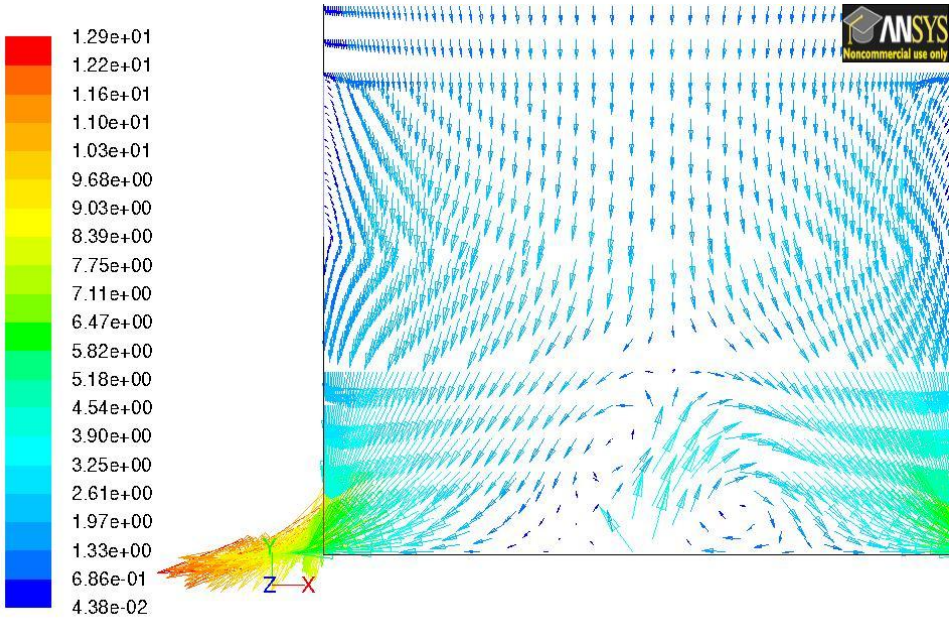

Figure 3.3 Velocity vectors of case two

3.2 Variations in Oxidizer Velocity

Having set the porosity in the particle zone to 0.5 and removed the y-component of the velocity for the fuel inlet, Figure 3.4 demonstrates that the oxidizer velocity makes a great deal of difference in the combustion of the biomass. In case one, seen in Figure 3.4(a), with an oxidizer velocity of 1.0 m/s, the temperature gradient creates a bubble rising from the lower left corner up and to the right. The area of maximum temperature is reached near the right fuel inlet and against the wall below the inlet. This temperature spike is then swept up and to the left in an arc, extending over half the gasifier. The

temperatures range from 337-462K under the bubble with maximum values of 549K reached at the right wall.

Case two has an oxidizer velocity of 5.0 m/s and shows a distinct change in the velocity gradient as seen in Figure 3.4(b). While an arched pattern is still present, all of it resides in the particle zone and the arc originates from the bottom of the gasifier. The maximum temperature exists at the bottom wall on the entire left side at 936K while the arc has a temperature of around 600K. Beneath the arc is an area of dramatically decreased temperatures (298-394K).

With the oxidizer velocity set at 15 m/s in case three, the temperature profile is much different, as seen in Figure 3.4(c). The increased velocity of the oxidizer flattens the temperature gradient even more, to an almost perfect horizontal line. The gradient also increases quickly to the maximum temperature (613K) that stretches from wall to wall before decreasing again. The majority of temperatures below the maximum line range from 330-560K, with the cooler temperatures dominating the area.

Investigating the mixture fraction in each of the cases can once again aid in the understanding of the combustion and gasification zones due to varying oxidizer velocity. This is shown in Figure 3.5. Similar to the findings from the varying porosity, areas below the high temperature gradients show increasing mixture fractions. Case one, shown in Figure 3.5(a), shows the same bubble-like pattern with a large area of high fuel mixture in the lower left corner. Figure 3.5(b) shows a steep gradient in the cooler temperature areas under the higher temperature arc that reaches a mixture fraction of 1.0 at the bottom of the gasifier for case two. Case three is illustrated in Figure 3.5(c) with a small triangle of unburned fuel at the center of the bottom wall of the gasifier with steep

gradients out, creating a slight peak at the top that can be seen in the temperature gradients of Figure 3.4(c).

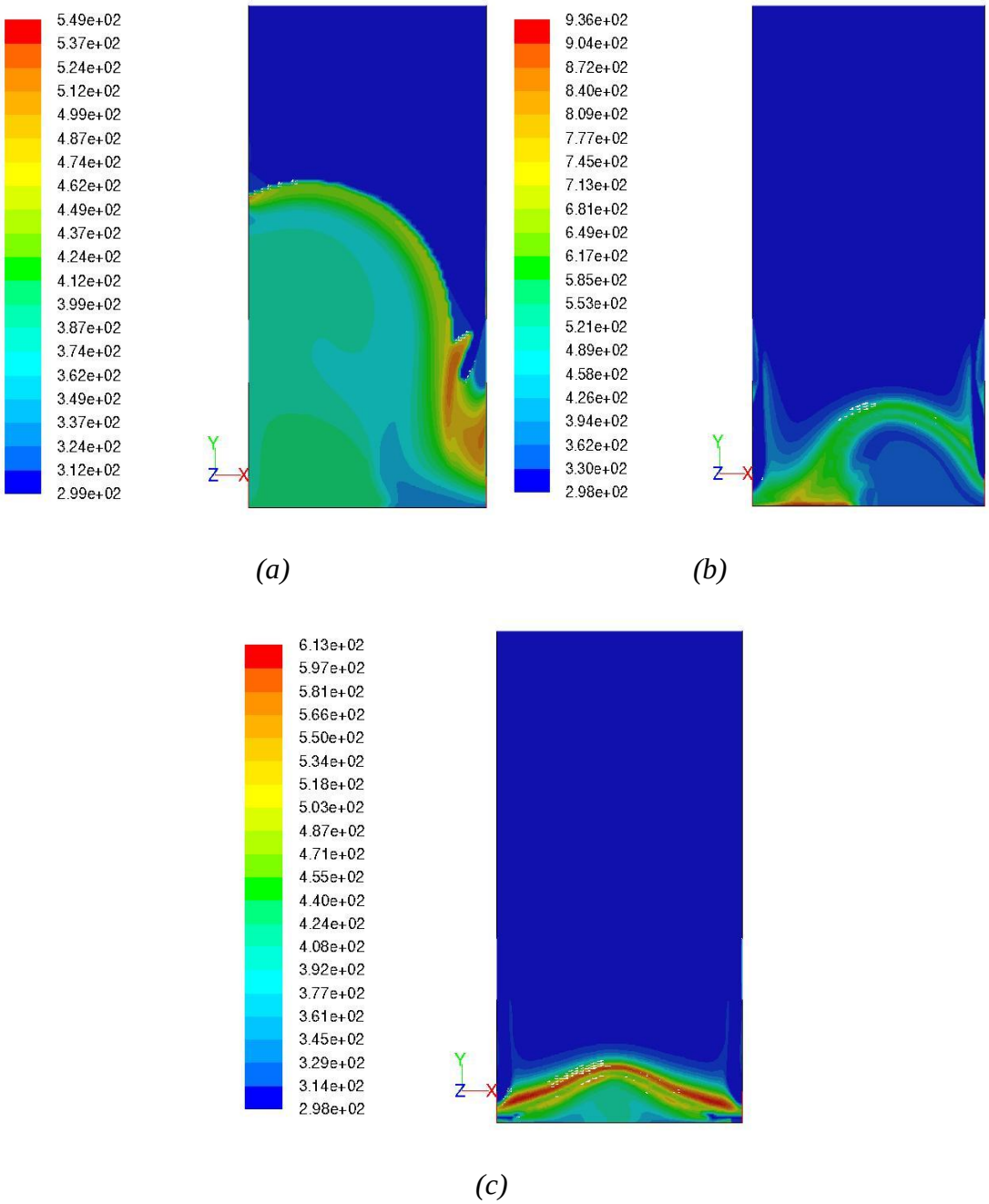

Figure 3.4 Temperature gradients at 1 m/s (a), 5 m/s (b), and 15 m/s (c)

The SCL can again be seen at the contour where the mixture fraction becomes greater than 0 and it continues in RFC until mean mixture fraction 0.75 when gasification begins. The temperature gradients show that these areas agree as they did in the variable porosity cases. The various bubbles and peaks created can be seen by the velocity vectors in Figure 3.6 through 3.8. The turbulence in the system is creating vortices within the flow due to the mixing inlet velocities and determines the shape of the combustion zone and gradients.

Figure 3.9 shows a progression of the velocity vectors for inlet velocity 1 m/s through the steady state computations. As seen, the first 50 iterations create two symmetric convection curls in the packed bed region with a higher velocity updraft in the center. After 100 iterations the solution is still symmetric and exhibits larger convection curls with high velocity updraft in the center. However, at 200 iterations, the curls are no longer as distinct with marked concentration of higher speeds towards the walls and again, increased updraft velocity in the center. At 200 iterations, a slight shift towards the left wall also begins to appear at the top of the updraft, accompanied by the shifting of the centers of each vortex. The left vortex has shifted up, while the right has shifted down. After 300 iterations the vortex on the right is almost completely non-existent and demonstrates an elongated flow pattern while the left vortex has remained circular and high. The updraft is similar in velocity magnitude to the solution at 200 iterations and shows an increase in the tilt to the left. At 500 iterations there is a dramatic increase in the left shift by the updraft and the formation of a large circular convection curl to the upper right. The left convection curl has shifted down and decreased in size and intensity. By the time the solution has converged at 1157 iterations, the developing right side convection curl has shifted towards the center and dominates the width of the gasifier.

There still appears a strong updraft at the center of the bottom, packed region, and a small, slightly faster curl in the lower left corner. These developments mirror the patterns found in the mixture fraction, with the hooking pattern following the upper edge of the large convection curl in the middle of the gasifier and the deposit of unburned fuel in the lower left corner. The clockwise direction of the large curl would suggest that the fuel and air are mixing more readily at the fuel inlet where we see the combustion zone begin.

To more fully understand the location of combustion, or even if it occurs, CO_2 output can be examined (Figure 3.10). Increased levels of CO_2 would be expected near the SCL for pure combustion. Tapering levels would be expected, moving forward from that line into the RFC. As seen in 3.10(a), the CO_2 pattern follows the same upward arc from right to left as the seen in the temperature and fuel gradients in 3.4(a) and 3.5(a), respectively. The CO_2 increases up to its maximum value at the points of highest temperature which is expected in the gasification and combustion zones. As the combustion at this velocity reaches a maximum temperature of 549K, the breakdown of such heavy hydrocarbons is not expected, and is not seen (Ulstad, 2010). The decrease in the CO_2 shown is due to the RFC and gasification which would leave more and more unburned fuel and volatiles.

Comparing the temperatures and CO_2 production from the second case (Figures 3.4(b) and 3.10(b)) shows a similar distribution. However, the temperatures achieved in this scenario are much increased with the combustion and gasification zone assumed to be in the 585 – 900K range. Inside this hook, the CO_2 increases as is expected for combustion and pyrolysis, then decreases as less and less fuel is burned. Some of the fuel is still being converted via RFC and once the mean mixture fraction approaches 0.75 (Figure 3.5(b)) with the temperatures hovering around 400K, the CO_2 fraction begins to

decrease. The temperatures are high enough for gasification, but not high enough for the breakdown or production of more CO_2.

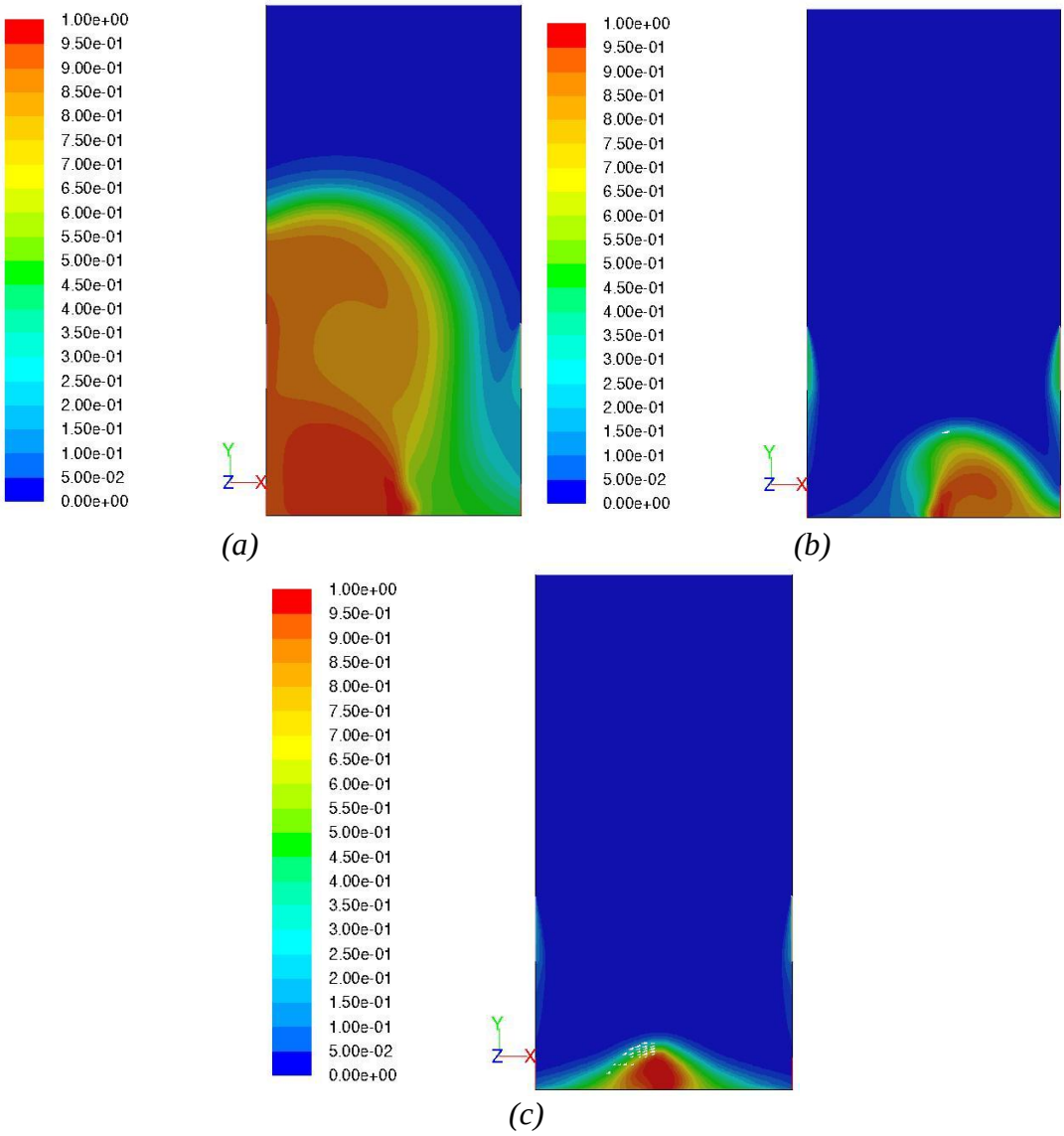

Figure 3.5 Mean mixture fractions for oxidizer inlet velocities 1 m/s (a), 5 m/s (b), and 15 m/s (c)

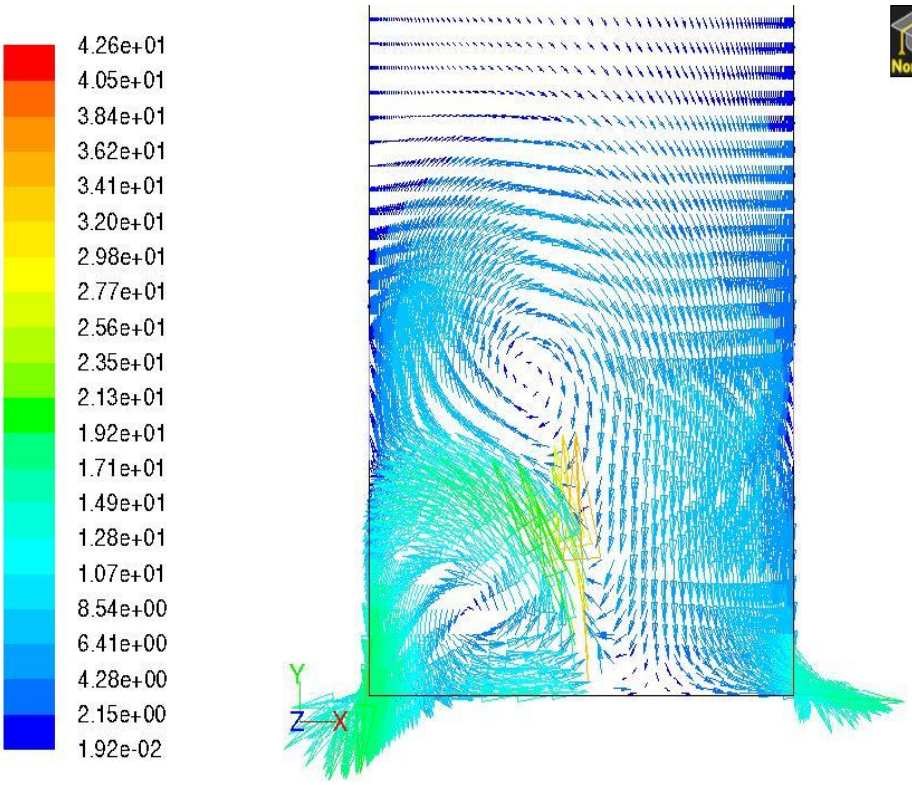

Figure 3.6 Velocity vectors for oxidizer velocity 1.0 m/s

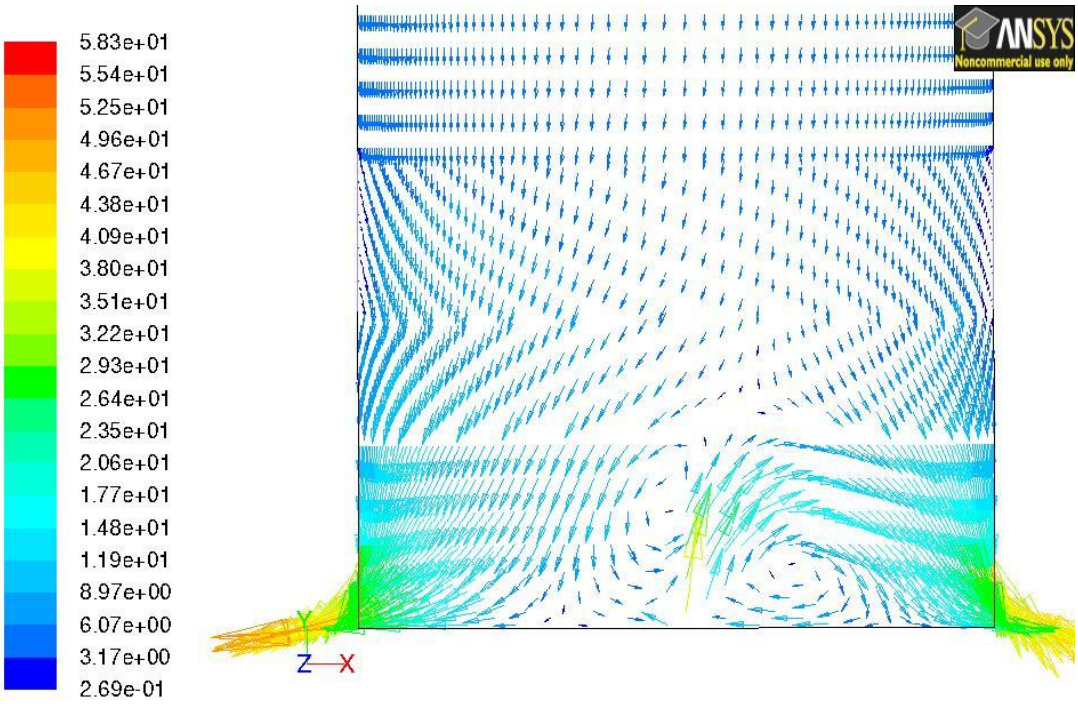

Figure 3.7 Velocity vectors for oxidizer velocity 5.0 m/s

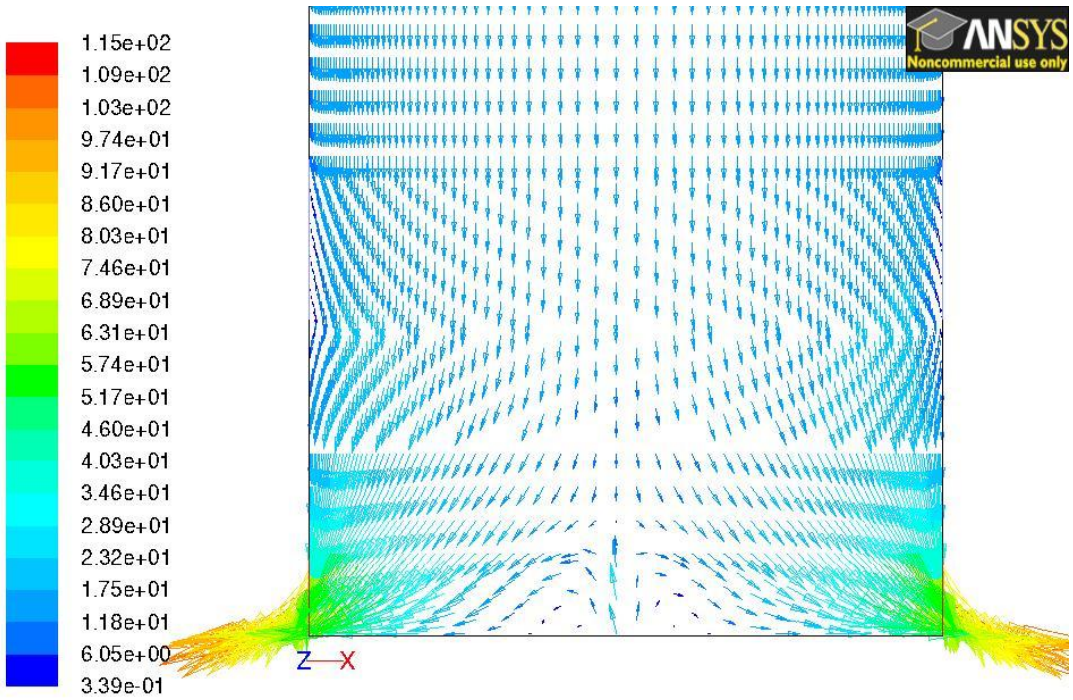

Figure 3.8 Velocity vectors of oxidizer velocity 15 m/s

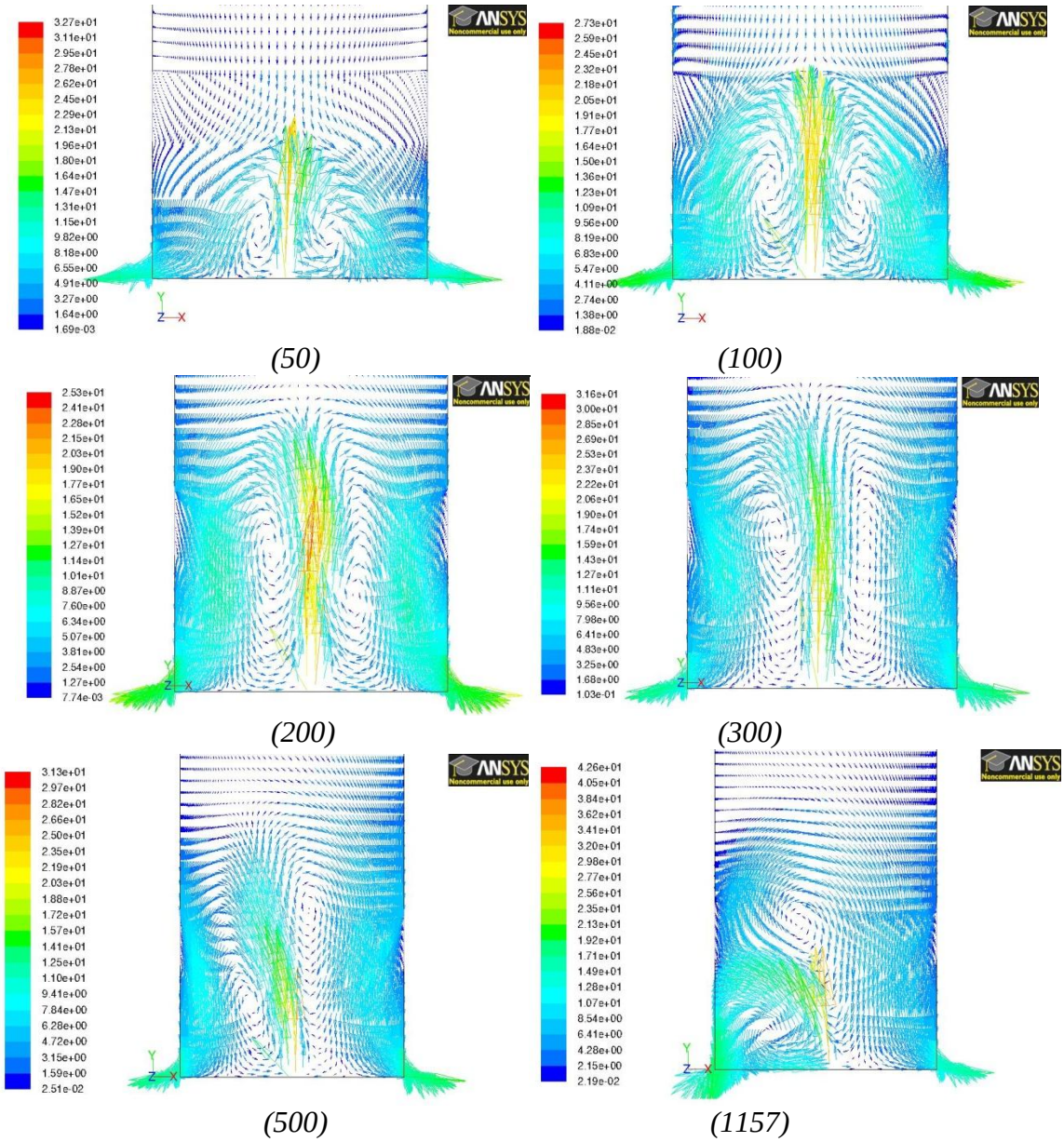

Figure 3.9 Iterations of 1 m/s solution, using velocity vectors

The velocity is increased to 15 m/s in the third case, as seen in Figure 3.10(c) and shows similar findings to the previous two cases. However, in this case the CO_2 production does not begin until the highest static temperature (613K) is achieved (Figure 3.4(c)). The maximum amounts of CO_2 are achieved in the areas of temperature around 455K and with a mean mixture fraction of 0.5. Although combustion does not appear to

begin until the maximum temperature has been reached in this case either, no pyrolysis leading up to the SCL is seen. The velocity of the oxidizer is such that it is pushing through the zone where pyrolysis would be expected before it has time to heat up or react with the material present. The maximum temperature is also in the zone that would break down CO_2, via char combustion (Equation 1.12) in fast-type pyrolysis (Ulstad, 2010).

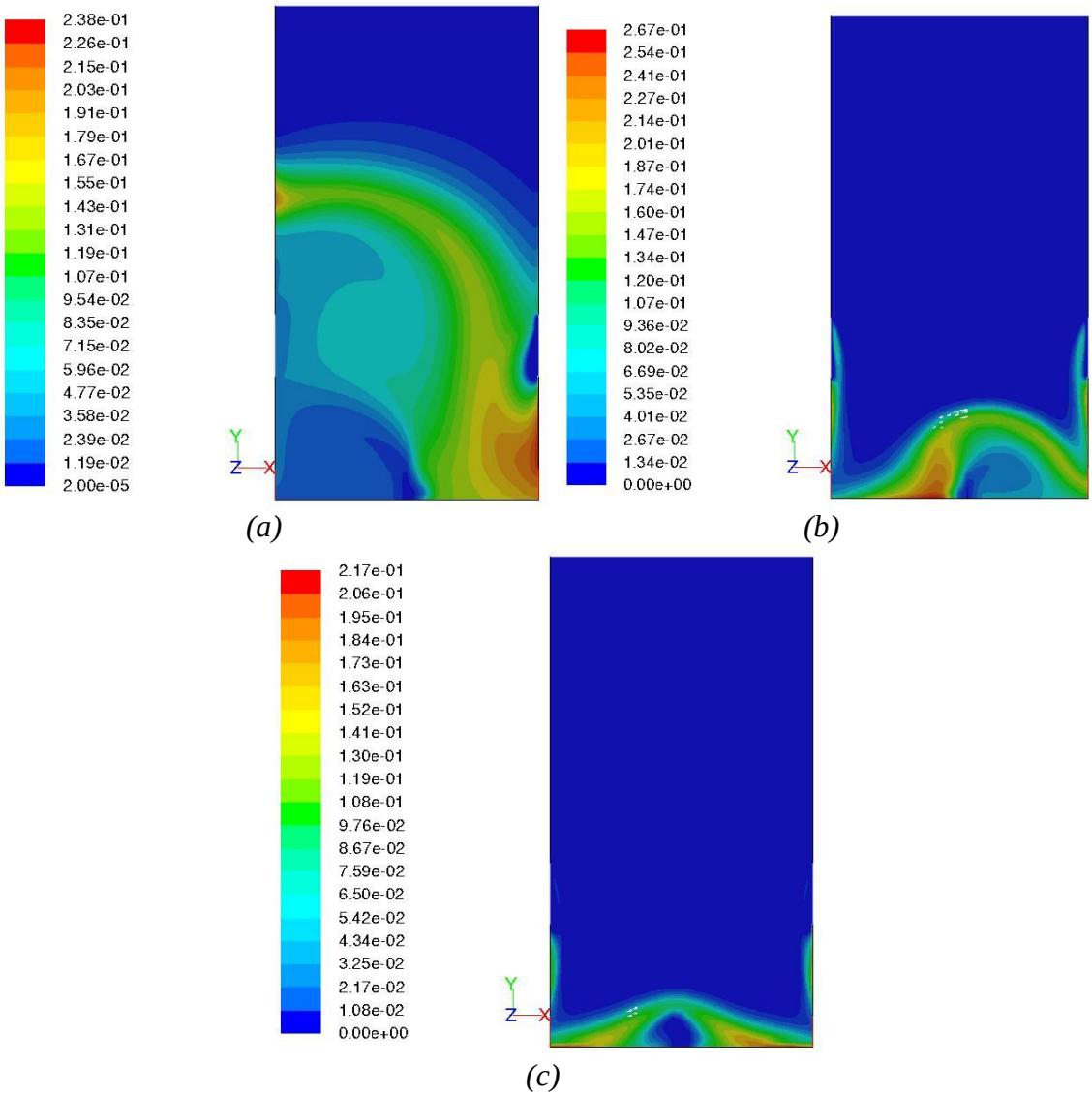

Figure 3.10 CO_2 fractions and oxidizer inlet velocities 1 m/s (a), 5 m/s (b), and 15 m/s (c)

3.3 Variations in Fuel Type

With the results from the last two tests, the porosity was kept at 0.5 and the oxidizer inlet velocity was set to 1.5 m/s with 1 kg/s fuel mass flow rates using both wood and seed corn as fuel. The temperature gradients for both of these cases can be seen in Figure 3.11. While the two cases have the same pattern for the temperature gradient, the temperatures are much higher in the case with seed corn fuel (1080K).

The overall shape of the gradient is the same and hooks up and to the right from the bottom left corner; the maximum temperature location is different. Figure 3.11(a) shows seed corn produces not only a hotter region than wood, but the hot region is located along the left bottom wall. The "hook" then maintains a range of 650 to 845K. The wood maximum temperature (678K) is spread out from the pressure outlet on the left up through the "hook" with a patch of the same high temperature located about 6" from the left fuel inlet (Figure 3.11(b)). This same small patch is seen in the corn figure but does not reach the maximum temperature. Although the wood maximum temperature is spread out throughout the "hook", the temperature range within is only 470-678K. While the temperatures of the "hook" are very different, the temperature under it, in both cases, is in the 300-400K range.

The mixture fraction can be seen for both of these cases in Figure 3.12. As expected, the patterns are similar for the mass fractions, as they were for the temperature distributions. It can be seen that small amounts of fuel are left unburned at the left fuel inlets while larger amounts are left entering from the right fuel inlet and grouped along the bottom right corner.

These findings are consistent with the varying porosity and oxidizer inlet velocity cases indicating that the cooler areas after combustion are filled with unburned fuel. The

different fuels also show the SCL at the 0 mean mixture fraction contour, with RFC continuing until gasification at mean mixture fraction 0.75.

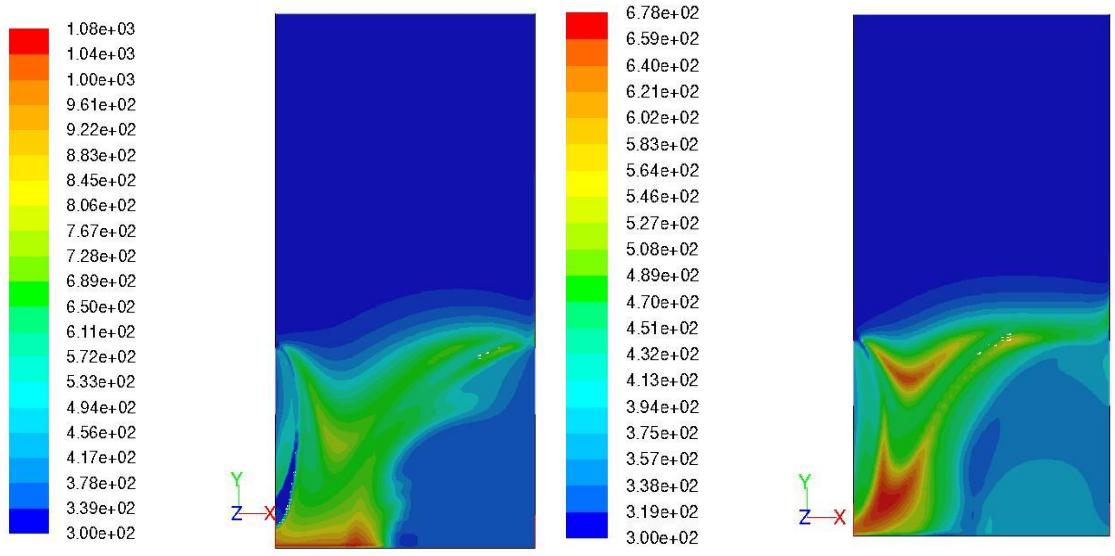

(a) *(b)*

Figure 3.11 Temperature gradients for (a) corn and (b) wood

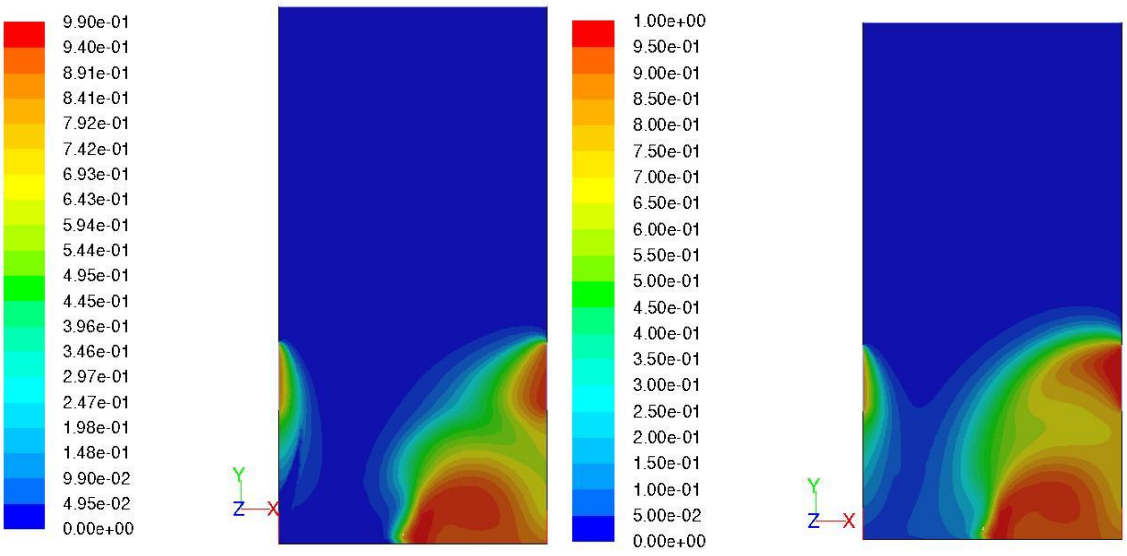

(a) *(b)*

Figure 3.12 Mean mixture fractions of (a) corn and (b) wood

CHAPTER 4

CONCLUSIONS AND FUTURE WORK

4.1 Conclusions

A computational model of a 2-dimensional fire tube was created in FLUENT to simulate the combustion and gasification of biomass materials with variable input parameters. Although the results from the tests are modeling the combustion of biomass, the results have implications on the gasification zone and process in a downdraft gasifier of this design.

Changing the porosity in the combustion and gasification zones (particle packing zones) indicated that a fuel with a packing density that correlates to a porosity of 0.5 would be the best. This porosity produced an even temperature gradient to allow for a larger and more thorough combustion and gasification zone.

Although it appears at first glance that case three, at 15 m/s, is a more complete combustion, an inlet oxidizer velocity of 1 m/s provides a larger combustion and gasification zone albeit with larger areas of unburned fuel. It was also shown that the 5 m/s velocity inlet produces both a smaller area of unburned fuel and smaller combustion and gasification zones. While the CO_2 output from each of these cases follows the temperature and mean mixture fraction patterns, the temperatures in the 1 m/s case (case one) show a substantial area where gasification can occur but not the breakdown of CO_2. This is not the case in the other two cases, where the temperature gradients are such that neither gasification nor CO_2 breakdown would occur in large quantities.

When comparing the different types of fuels, it is evident that while the corn has smaller areas of unburned fuel (Figure 3.11(a)), the wood appears to have large portions

of the combustion and gasification zones within a temperature range of 450-525K, which are within the acceptable temperatures for gasification and pyrolysis to occur.

These results indicate that the non-premixed combustion model of FLUENT works for modeling the combustion and gasification zones of the downdraft gasifier. It was also shown that oxidizer inlet velocities of less than 5 m/s would be best for this combination of parameters and for materials that have a packing density of around 0.5. While both seed corn and wood can be used in this model, the wood fuel appears to have a lower temperature gradient with a larger probability of gasification.

4.2 Future Work

In the future, user-defined functions can be implemented into this model to more accurately model the composition of the various biomass materials tested. A more accurate model would require a complex chemical kinetics study to capture all of the sub-species, reactions, reactions rates, and endo- or exothermic data. This information would increase the validity of the model and improve results for specific biomass fuels.

Also, a more defined thermal conduction equation could be created to model the heat transfer between the particles, their volatiles, and the oxidizer, to be used in this model. This would serve to more distinctly model the gasification zone without the necessary kinetics research described above.

Further work could be done to introduce injections into the model to predict what each particle would do in the system. While this was attempted in this model, the combination of the density of the particle and being dropped from the top of the gasifier with gravity caused the particle to have a residence time of around 4 seconds. In this time the particle was not able to interact with the continuous functions of the gasifier and only produced a mild rise in temperature (from 300K to 309K). In some cases the temperature

was able to reach 400K, but this was unable to show any changes in density, mass, or species fraction, indicating that no reactions were taking place up to this temperature.

REFERENCES

ANSYS. (2009, 01 23). ANSYS FLUENT 12.0 Technical Guide. (12.0).

Atnaw, S. M., & Sulaiman, S. A. (2009). Modeling and Simulation Study of Downdraft Gasifier Using Oil-Palm Fronds. *Proceeding of ICEE 2009 3rd International Conference on Energy and Environment* (pp. 284-289). Malacca, Malaysia: ICEE.

Babu, B., & Chaurasia, A. (2003). Modeling for pyrolysis of solid particle: kinetics and heat transfer effects. *Energy Converstion & Management*, 2251-2275.

Ciegis, R., & Starikovicius, V. (2002). Mathematical Modeling of Wood Drying Process. *Mathematical Modeling and Analysis*, 177-190.

Cornejo, P., & Farias, O. (2011). Mathematical Modeling of Coal Gasification in a Fluidized Bed Reactor Using a Eulerian Granular Description. *International Journal of Chemical Reactor Engineering*, A2.

Cuoci, A., Garavelli, T., A, F., Grana, R., Pierucci, S., Ranzi, E., et al. (2009). Mathematical modeling of gasification and combustion of solid fuels and wastes. *Chemical Engineering Transactions*, 989-994.

Huang, H.-J., & Ramaswamy, S. (2009). Modeling Biomass Gasification Using Thermodynamic Equilibrium Approach. *Applied Biomechical Biotechnology*, 193-204.

Paes, T. (2005). *Modeling for control of a biomass gasifier.* Eidhoven: Technische Universiteit Eindhoven.

Ragland, K., & Aerts, D. (1991). Properties of Wood for Combustion Analysis. *Bioresource Technology*(37), 161-168.

Reed, T., & Desrosiers, R. (1979). Retrieved March 10, 2011, from Wood Gas: www.woodgas.com

Stull, R. L. (2003). *Coal Analysis (Proximate and Ultimate) from the Delta Junction Area, Alaska.* Fairbanks, AK: State of Alaska Department of Natural Resources.

The University of Iowa. (2007). Pioneering Technology for Utilizing Biomass Fuels.

U.S. Department of Energy. (2011). *Independent Statistics and Analysis*. Retrieved February 10, 2011, from U.S. Energy Information Administration: www.eia.doe.gov

U.S. Department of Energy. (n.d.). *The Energy Lab*. Retrieved February 10, 2011, from National Energy Technology Laboratory: www.netl.doe.gov

Ulstad, J. (2010). *Gas Evolution of Corn Kernels, Oat Hulls, and Paper Sludge from Biomass Gasification.* Iowa City, IA: University of Iowa.

Watanabe, H., & Otaka, M. (2006). Numerical simulation of coal gasification in entrained flow coal gasifier. *Fuel*, 1935-1943.

Wen, C., & Chaung, T. (1979). Entrainment Coal Gasification Modeling. *Industrial & Engineering Chemistry Process Design and Development*, 684-695.

Yilmaz, H., Perumalsamy, S., Oeljeklaus, G., Gorner, K., Klasen, T., Benim, A. C., et al. (2010). CFD Analysis of a Large Scale Entrained-Flow Gasifier for IGCC Power Plants. *7th International Conference on Multiphase Flow*. Tampa, FL: ICMF.